

## SUPPORTING INFORMATION

**Table S1. Top ten ranked clusters of docking poses for the ‘open’ ATG4B (ATG4B (O)).**

Cluster rank	Lowest Binding Energy	Mean binding energy	Number of conformations	Region
	$\Delta G$ (kcal/mol)	$\Delta G$ (kcal/mol) in the cluster		
1	-9.69	-9.15	11	1
2	-9.11	-8.52	8	1
3	-9.06	-8.54	9	1
4	-8.81	-8.70	3	1
5	-8.73	-8.73	1	1
6	-8.43	-8.22	11	1
7	-8.31	-7.69	5	2
8	-8.21	-8.03	2	1
9	-8.13	-8.13	1	1
10	-8.01	-8.01	1	1

**Top ten ranked clusters of docking poses for the ‘closed’ ATG4B (ATG4B (C)).**

Cluster rank	Lowest Binding Energy	Mean binding energy	Number of conformations	Region
	$\Delta G$ (kcal/mol)	in the cluster		
1	-8.15	-7.75	23	1
2	-7.75	-7.35	9	1
3	-7.67	-7.46	3	1
4	-7.47	-7.43	2	1
5	-7.45	-7.24	2	1
6	-7.41	-6.98	4	2
7	-7.31	-7.27	2	1
8	-7.26	-7.26	1	3
9	-7.25	-7.25	1	3
10	-7.23	-7.19	2	1

**Top ten ranked clusters of docking poses for LC3.**

Cluster rank	Lowest Binding Energy	Mean binding energy	Number of conformations	Region
	$\Delta G$ (kcal/mol)	in the cluster		
1	-7.52	-7.16	3	1
2	-7.44	-7.21	3	1
3	-7.28	-6.89	11	2
4	-7.04	-6.98	3	1
5	-6.95	-6.69	30	3
6	-6.88	-6.54	4	3
7	-6.81	-6.47	3	1
8	-6.70	-6.70	1	2
9	-6.64	-6.64	1	1
10	-6.59	-6.48	6	2

**Top ten ranked clusters of docking poses for the open/active form of ATG4A.**

Cluster rank	Lowest Binding Energy	Mean binding energy	Number of conformations	Region
	$\Delta G$ (kcal/mol)	in the cluster		
1	-9.70	-9.17	15	1
2	-9.10	-8.60	3	1
3	-9.01	-8.60	8	1
4	-8.96	-8.63	27	1
5	-8.69	-8.66	3	1
6	-8.47	-8.17	8	1
7	-8.34	-8.08	5	1
8	-8.23	-8.23	1	1
9	-8.13	-8.13	1	1
10	-8.11	-8.11	1	1

Clusters are ranked by the lowest binding energy  $\Delta G$  (kcal/mol) in each cluster. The mean binding energy  $\Delta G$  (kcal/mol) is calculated by averaging the binding energy of all poses in a cluster. The spatial “regions” that indicate the locations of the individual clusters are labeled in Figures 3C, 3D, 3E, and S2.

## SUPPLEMENTAL FIGURE LEGENDS

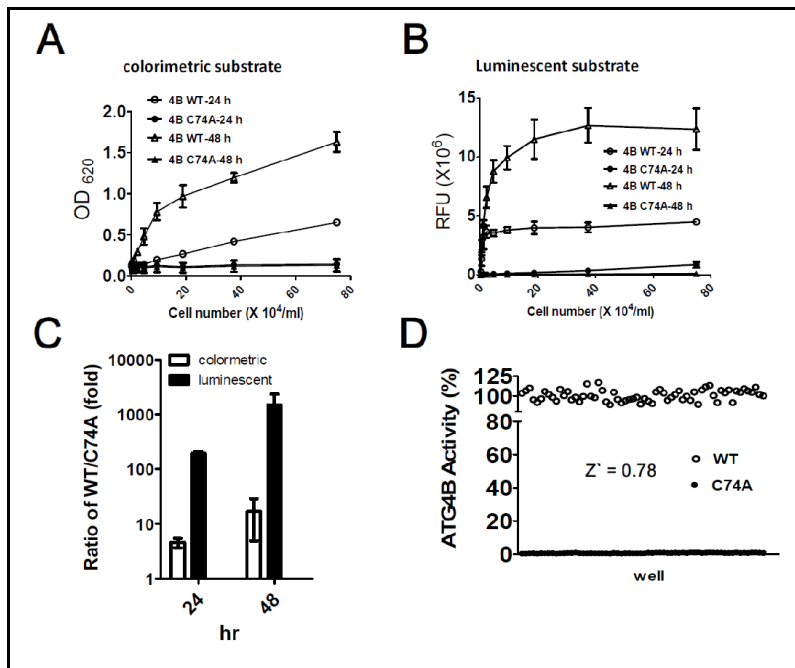


**Figure S1. Characterization of Yeast Based ATG4B Reporter Assay for HTS.** (A) Two-fold serial titrated yeast that harbored the LC3 reporter with wild type ATG4B (WT) or catalytic mutant (C74A) expression vector and reporter vector were seeded into a 384-well plate for 24 or 48 h. The substrate of  $\beta$ -galactosidase X-gal (80  $\mu$ g/ml) was included in the SD medium for the colorimetric assay. (B) Beta-Glo was added into each well as (A) at 24 or 48 h to optimize the yeast concentration for the luminescent substrate. (C) Yeast that harbored the wild type (WT) ATG4B and catalytic mutant (C74A) were used to determine the ratio of signal (WT)/background (C74A) and compare the sensitivity between the colorimetric and luminescent substrates. (D) Forty  $\mu$ l of yeast reporter cells ( $1.5 \times 10^4$  cells/ml) as previously described were seeded into a 384-well white plate for 24 h. Ten  $\mu$ l of the luminescent substrate Beta-Glo was added to each well, and the luminescent signal was read to determine the ATG4B activity. The luminescent signal between the wild type (WT) ATG4B and catalytic mutant (C/A) was used to determine the assay robustness ( $Z'$  factor: 0.78). The results are expressed as the mean  $\pm$  SEM from 3 individual experiments.

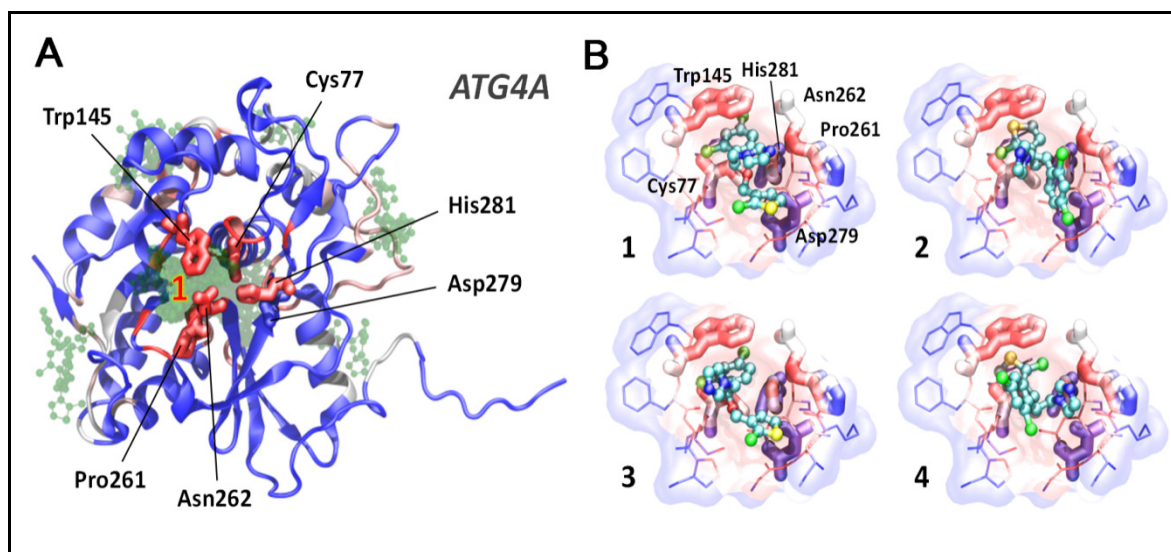


**Figure S2. Tioconazole also Docks into the Active Site of ATG4A.** The 100 docking poses in the open/active structure of ATG4A are obtained from AutoDock (A), and the lowest energy pose in each of the four highest scored clusters (rank-ordered by their lowest energy pose) is shown in (B). The spatial “regions” that indicate the locations of the clustered poses identified by AutoDock (Table S1) are labeled (red number). The open/active forms of the ATG4A structure are constructed by the SWISS-MODEL web server (Biasini et al., 2014) using the ATG4B open form (PDB: 2Z0D) as the structural template. The color scheme is the same as shown in Figure 2. Note that pose 1 here is almost in the same orientation as pose 1 (Figure 3f) for the open form of ATG4B. We selected the highest ranked four poses shown in panel B for further MD simulations. The results demonstrate that the ligands of poses 1, 3 and 4 remain at the binding pocket throughout the entire 100 ns of simulations. The docking pose for the pose 1 ligand after the 61st ns of the simulation resembles pose 2 in the simulation for ATG4B (O) except for a different direction where the imidazole ring points. For pose 2, the ligand leaves the binding pocket after 75.8 ns. For pose 4, although the ligand stays around the binding pocket throughout the 100 ns simulations, it notably changed its binding orientation and position.

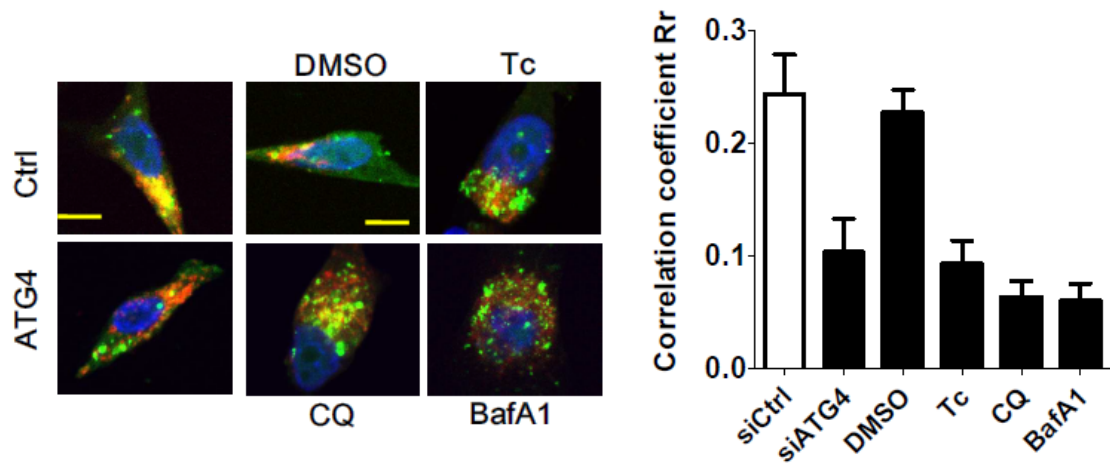


**Figure S3. Effects of Tioconazole on fusion between autophagosome and lysosome.** H4 cells expressing GFP-LC3 and RFP-Lamp1 were treated with Tc for 6 h and fixed to observe colocalization of GFP-LC3 and RFP-Lamp1 with confocal microscopy. The GFP-LC3 colocalized or surrounded by RFP-Lamp1 was identified as fusion between autophagosomes and lysosomes. The colocalization coefficients of images were quantified by the Zeiss LSM 710 Software and shown in right panel. Bar: 20  $\mu$ m.

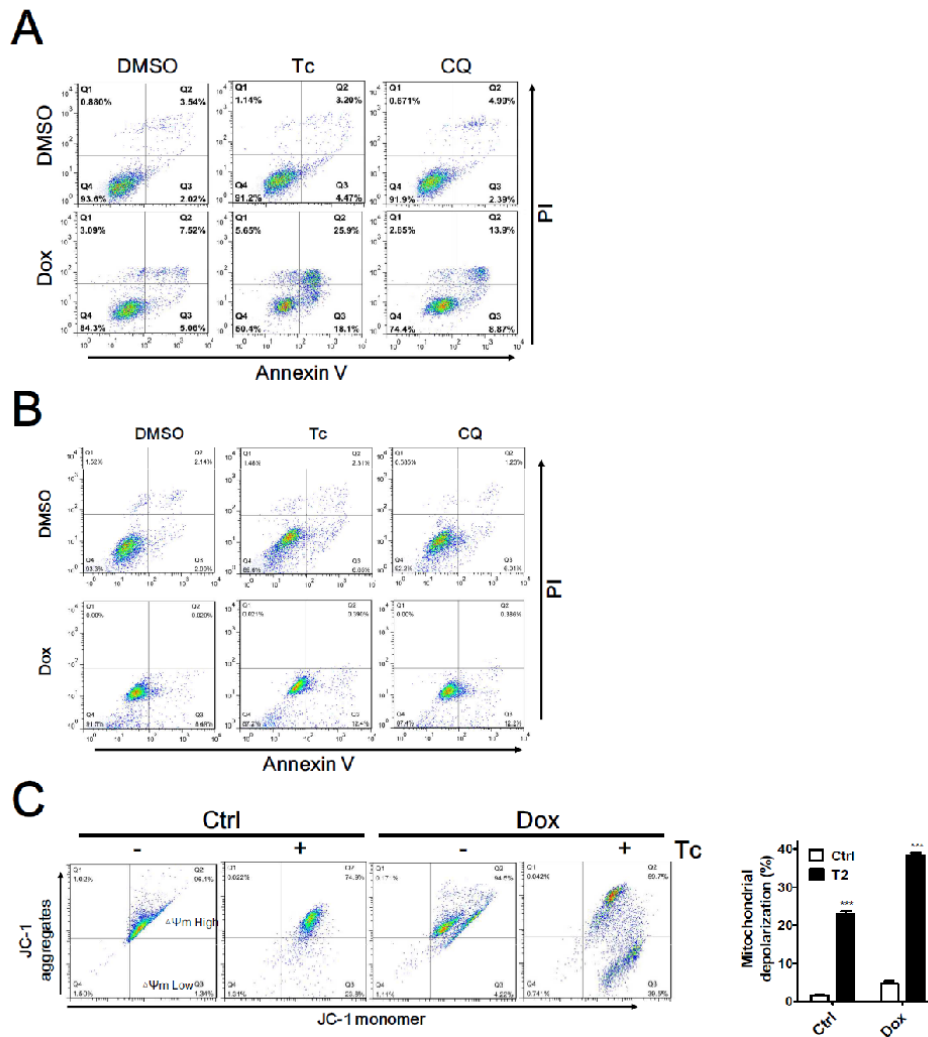


**Figure S4. Tioconazole Enhanced Dox-Induced Apoptosis in Cancer Cells.** (A) H4 and (B) MDA-MB-231 cells treated with Dox (1  $\mu$ M) for 24 h in the presence or absence of TC (40  $\mu$ M) were harvested and stained with PI/AV. The early (PI<sup>-</sup>/AV<sup>+</sup>) and late (PI<sup>+</sup>/AV<sup>+</sup>) apoptotic cells were analyzed via flow cytometry. (C) H4 cells were treated with Dox (1  $\mu$ M) for 24 h in the presence or absence of Tc (40  $\mu$ M) and stain with JC-1. The JC-1 stained cells were utilized to determine the mitochondria membrane potential with flow cytometry. The representative data and quantitative results are shown in the left and right panels, respectively. The results are expressed as the mean  $\pm$  SEM from 3 individual experiments.

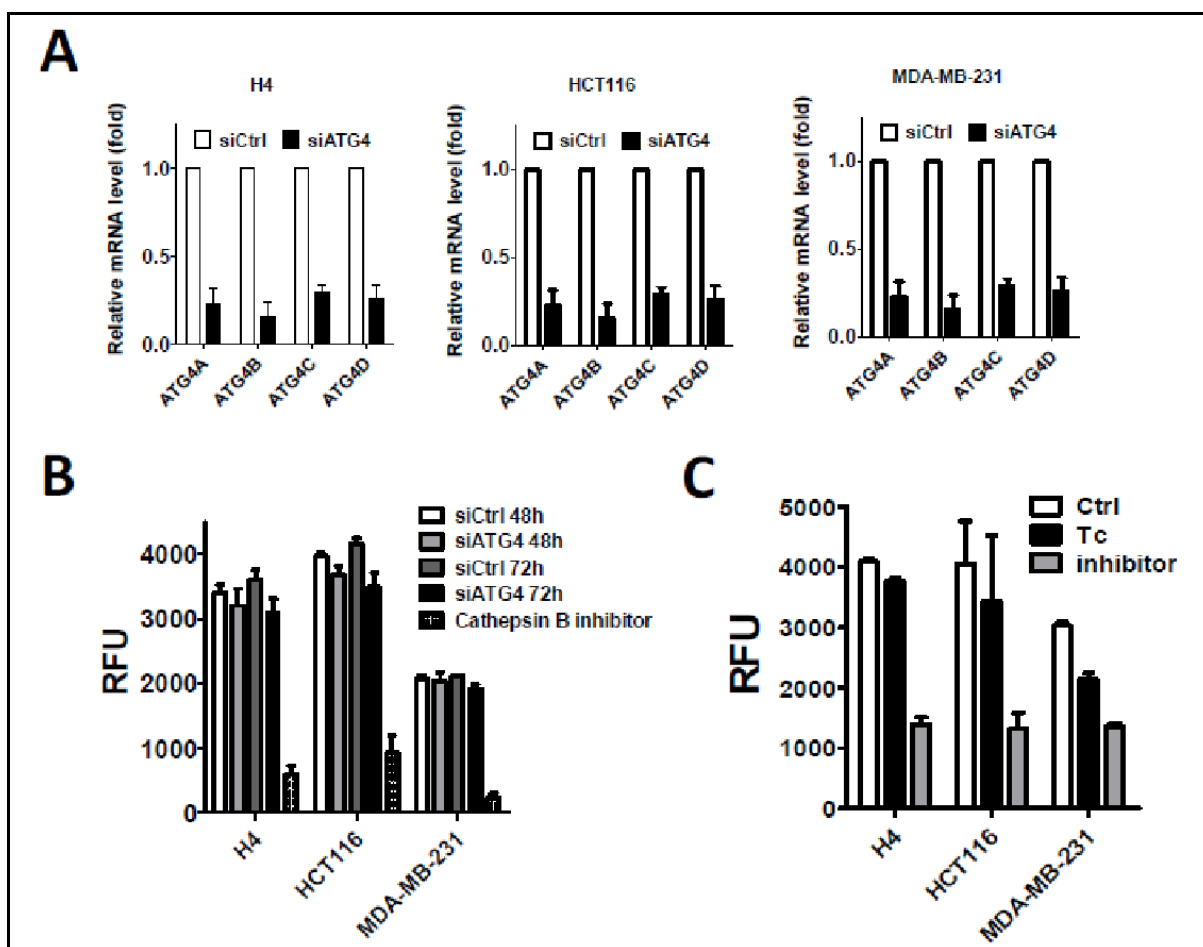
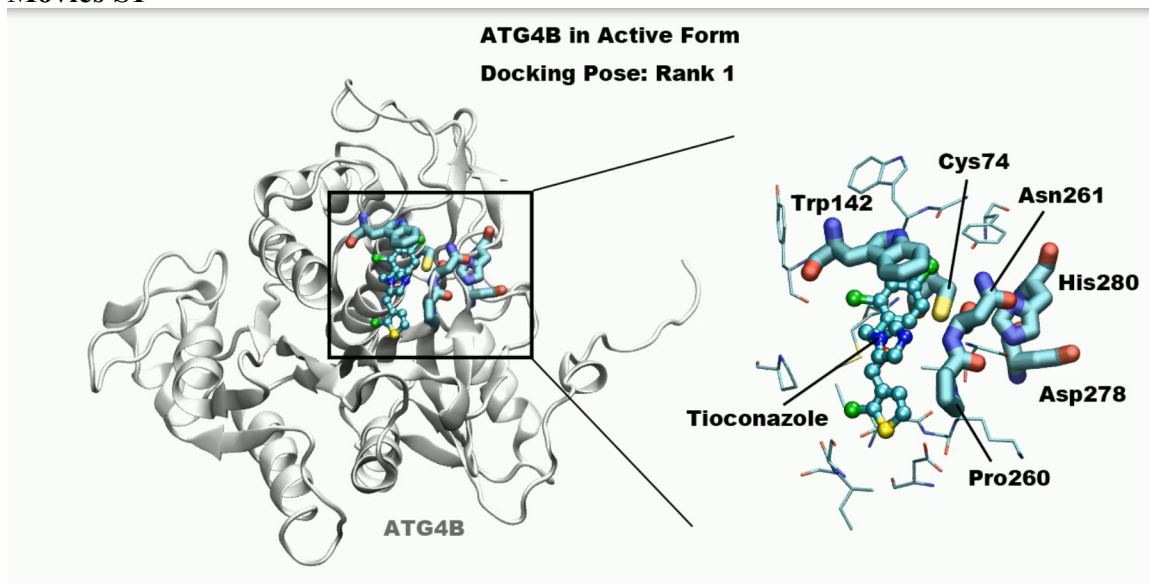


**Figure S5. The Effects of Silencing ATG4 and tioconazole on cathepsin B activity.** (A) H4 , HCT116 and MDA-MB-231 cells were transfected with 5 nM non-targeting siRNA (Ctrl) or siRNA against *ATG4* family members (ATG4) for 48 h. The knockdown efficiency of ATG4 was verified with real time PCR. (B)  $10^5$  of the ATG4 silenced cells were lysed to measure cathepsin B activity. Cathepsin B inhibitor is used a control. (C) H4, HCT116 and MDA-MB-231 cells were treated with tioconazole (40  $\mu$ M) for 6 h and equal amount cells were lysed to measure cathepsin B activity.

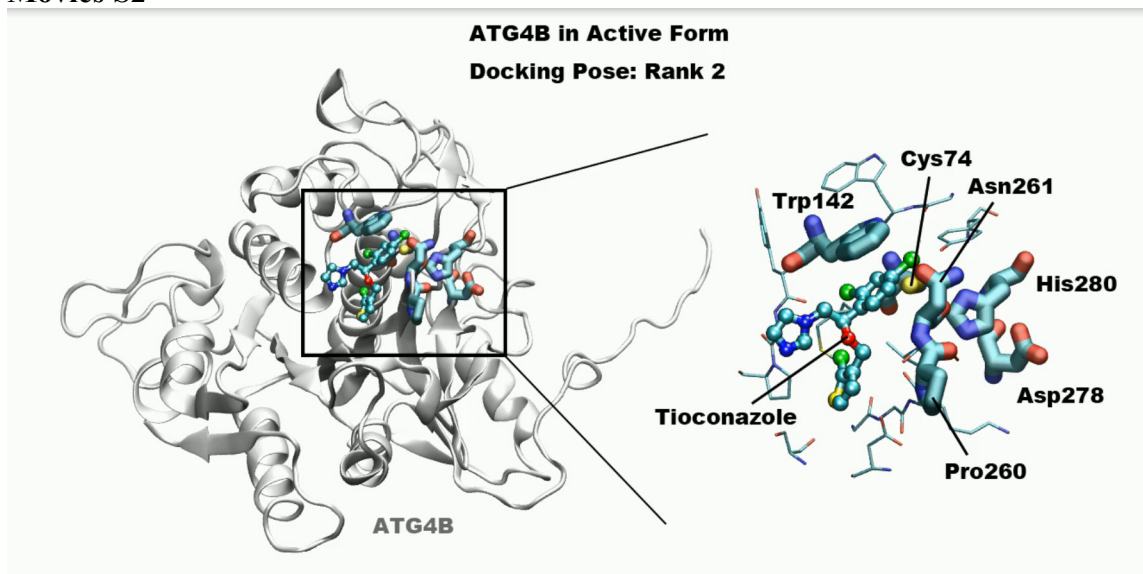
## SUPPLEMENTAL MOVIES

Movies S1 through S4 show the MD simulation trajectories for tioconazole docked into the active site of an isolated ATG4B in poses 1, 2, 3 and 6, respectively. Movies S5 and S6 show the MD trajectories starting from the rank 1 poses of tioconazole for ATG4B in the closed form and LC3. All the movies can be downloaded online (<http://dyn.life.nthu.edu.tw/Tioconazole/movie>)

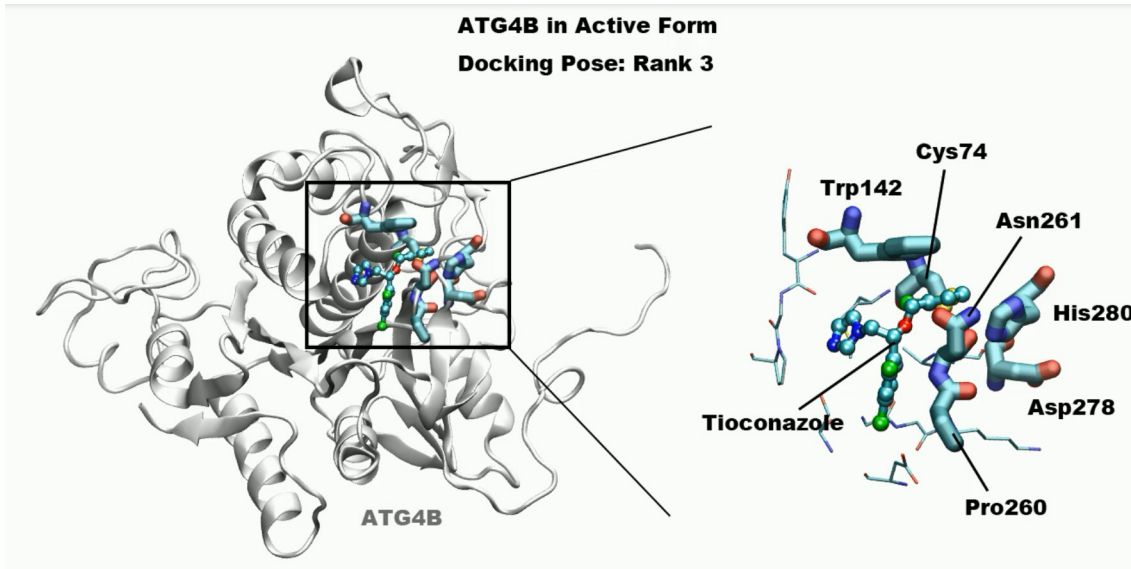
### Movies S1



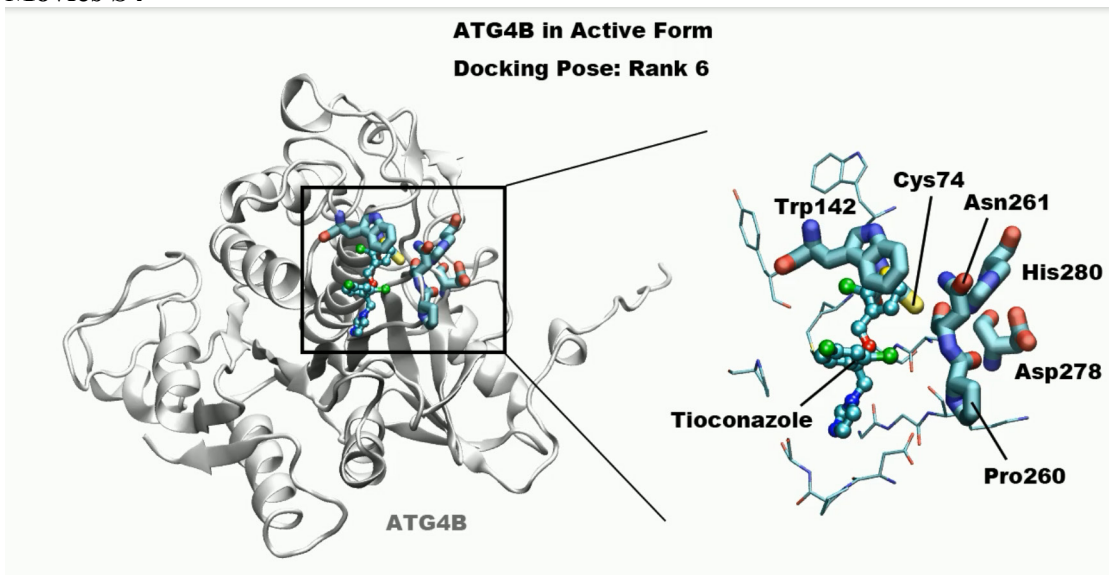
### Movies S2



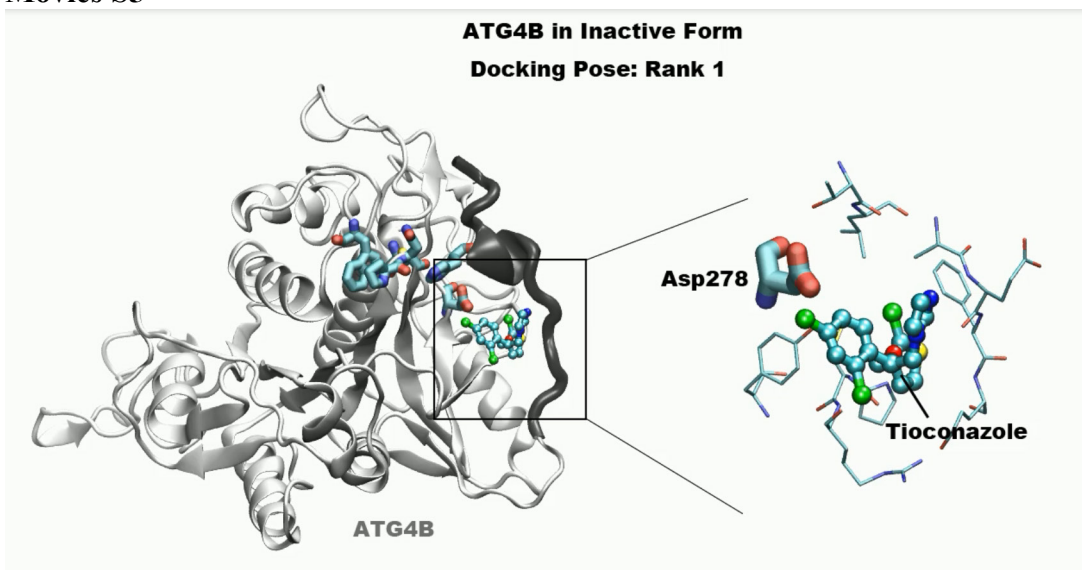
### Movies S3



### Movies S4



### Movies S5



## SUPPLEMENTAL EXPERIMENTAL PROCEDURES

### Structure Preparation

High-resolution structures of ATG4B alone (PDB code: 2CY7) and in complex with its substrate protein LC3 (PDB code: 2Z0D) were retrieved from the Protein Data Bank, respectively. ATG4B alone adopts a ‘closed’ (and inactive) conformation in which the N-terminal tail of ATG4B masks the exit of the active site, while an adjacent substrate-binding residue, Trp142, forms close contacts with Pro260 in the regulatory loop (G257 – A263), as well as with Tyr8 in the N-terminus [1]. The Trp142-Pro260 interaction (Figure 3B) shields off LC3 docking into the active site, whereas Trp142-Tyr8 stacking stabilizes the closed conformation. In the ATG4B-LC3 complex, ATG4B adopts an open/active conformation in which (A) the tip of the C-terminus of LC3, with the last 4 residues cleaved, is bound to the ATG4B active site centered with a catalytic cysteine, Cys74, and (B) a second LC3, a translated/rotated copy of the LC3 substrate present in one of the neighboring asymmetric units, holds the N-terminus of ATG4B open to un-mask the active site (Figure 3A). For the latter, the authors had authenticated the seizure of ATG4B N-terminus by N-LC3 in the solution state via NMR experiments [2]. To simulate the wild-type ATG4B, the mutation H280A, which facilitates the growth of stable crystals in the complex structure (2Z0D), is mutated back to histidine *in silico*. Missing residues in protein structures are patched by Discovery Studio and PDB Swiss Viewer prior to the docking experiments and subsequent simulation studies. All positions of hydrogen atoms and the missing residues are optimized via energy minimization using an AMBER16 ff14SB force field [3].

### Preliminary Drug Screening and Advanced Docking

We compiled a library containing 1312 drugs which are included in the FDA-approved drugs library from the company MedChem Express (MCE). The 3D structures of the drugs were modeled by the software, Balloon [4, 5], and some failed to be modeled were collected from the PubChem database [6]. Vina [7] was used to perform the *in silico* drug screening with the docking box covering the entire structure of ATG4B and at most 20 poses were allowed to be generated for each drug. Poses obtained from Vina for a given drug were further clustered using a cutoff of 10 Å. Any cluster that (1) contains more than 8 poses and (2) has an averaged (over all the poses in the cluster) distance from the active site (centered at the catalytic Cys74) less than 5 Å was selected. Then, only the poses whose closest atom is < 5 Å from the active site would be kept, which resulted in 1613 selected poses for 242 unique drugs. Among these poses, only those that originally ranked the first in their corresponding drugs according to the Vina-defined energy were kept. These 142 best-ranked poses, each representing a unique drug, were re-ranked based on the Vina-defined binding affinity, and the top 100 drugs were subject to further body-temperature explicit solvent (see below) MD simulations for stability and binding free energy evaluations (see below).

The most potent drug, screened from docking, MD simulation, biochemical and cellular assays, was subject to advanced docking for us to examine its atomic interactions with active site residues. We used AutoDock 4.2 [8] with elaborated energy-term-reweighting scheme [9] for this purpose. 100 poses were generated by initiating the docking in different starting conditions. The charge parameters are obtained from AMBER16 ff14SB [3] for proteins and am1bcc [10] for ligands. We use a scoring function with solvation parameters obtained from a robust regression analysis, which indicated the highest accuracy in the docking poses and energy evaluations among 16 scoring functions for a set of 1427 complexes [9]. All nonpolar hydrogens in the proteins and ligand are removed, and their charges are merged to adjacent carbon atoms via AutoDockTools. The grid boxes are adjusted to cover the entire protein structure, with a grid size of 0.375 Å. Maximal evaluations and the population size of individuals are set to 25,000,000 and 300, respectively. One hundred docking runs are performed for each examined system, including the open/closed forms of ATG4B and LC3. Other parameters are set as default values.

### Body-temperature Explicit Solvent Molecular Dynamics (MD) Simulations

MD simulations were performed using AMBER16 package. The ff14SB force field [3] was used for proteins, and the GAFF force field [11, 12] supported by an am1bcc charge method [10] was used for the ligand. TIP3P water model was used to solvate the system, and sodium and chloride ions were added to neutralize the system. For FDA-approved drug screening, the systems were first energy minimized for 1000 steps, heated to 320K in

NVT ensemble for 50 ps, and then density equilibrated at 310 K and 1 bar in NPT ensemble for another 50 ps. The C $\alpha$  atoms of the protein were restrained with a force constant of 100 kcal/mol/Å<sup>2</sup> during these three steps. After this, each drug was performed a 10 ns production run in the same condition as the NPT equilibrium except that the restraints were removed.

We further rank the top 100 drugs derived from the docking results based on their binding stability that is assessed by explicit solvent MD simulations, at body temperature, on two physical quantities. The first one is the root mean square fluctuations (RMSF) of the distances between a given drug to the ATG4B's active site. The second one is MM/GBSA-defined binding energy. For MM/GBSA calculation, the GBn model with modified parameters was used (igb=8), and the corresponding atom radii were adjusted (mbondi3 for PBRadii). All the snapshots sampled from the explicit solvent MD runs were taken for the GB energy calculation for each drug. For those drugs that left the binding site in ATG4B in the 10 ns simulations were ranked by how early they left by >10 Å (the earliest ranks the lowest) and ranked after those that did not leave their original pockets. For those that stay in the pocket throughout the 10ns simulation, they were ranked by the joint effect of the average RMSF and a normalized GBSA energy. The average RMSF for a drug is the average RMSF over all the heavy atoms of the ligand, and a normalized GB binding energy is the GB energy for a drug divided by the number of heavy atoms in the drug. The final rankings were determined by the sum of the rank per the average RMSF and the rank by normalized GB binding energy.

For the specific assessment of the binding stability for tioconazole docking poses, the protein-ligand complex or protein alone systems were first minimized with 6000 steps, with ligand restrained during the process (using a force constant of 500 kcal/mol/Å<sup>2</sup>) if it was present. The minimized structures, with or without tioconazole, were subsequently heated for 10 ps in the NVT ensemble with both protein and ligand lightly restrained (10 kcal/mol/Å<sup>2</sup>), followed by a 110 ps simulation in the NPT ensemble with only ligand being restrained (10 kcal/mol/Å<sup>2</sup>). Finally, the production runs for an unrestrained system were performed in the NPT ensemble. For all the simulations described above, the Langevin thermostat with a collision frequency of 2 ps<sup>-1</sup> was used for the temperature control and the Berendsen barostat for the pressure maintenance. The full electrostatic energy was calculated by Particle Mesh Ewald. The non-bonded distance cutoff was set to 10 Å. The ion concentrations were adjusted to the concentrations used in the experiment. A time step of 2 fs was used for all simulations. Trajectory visualization and analyses was carried out using VMD 1.9.2 software [13], pytraj [14], and in-house programs.

## SUPPLEMENTAL REFERENCES

1. Sugawara K, Suzuki NN, Fujioka Y, et al. Structural basis for the specificity and catalysis of human Atg4B responsible for mammalian autophagy. *J Biol Chem.* 2005; 280:40058-65.
2. Satoo K, Noda NN, Kumeta H, et al. The structure of Atg4B-LC3 complex reveals the mechanism of LC3 processing and delipidation during autophagy. *EMBO J.* 2009; 28:1341-50.
3. Maier JA, Martinez C, Kasavajhala K, et al. ff14SB: Improving the Accuracy of Protein Side Chain and Backbone Parameters from ff99SB. *J Chem Theory Comput.* 2015; 11:3696-713.
4. Puranen JS, Vainio MJ, Johnson MS. Accurate conformation-dependent molecular electrostatic potentials for high-throughput in silico drug discovery. *J Comput Chem.* 2010; 31:1722-32.
5. Vainio MJ, Johnson MS. Generating conformer ensembles using a multiobjective genetic algorithm. *J Chem Inf Model.* 2007; 47:2462-74.
6. Kim S, Thiessen PA, Bolton EE, et al. PubChem Substance and Compound databases. *Nucleic Acids Res.* 2016; 44:D1202-13.
7. Trott O, Olson AJ. AutoDock Vina: improving the speed and accuracy of docking with a new scoring function, efficient optimization, and multithreading. *J Comput Chem.* 2010; 31:455-61.
8. Morris GM, Huey R, Lindstrom W, et al. AutoDock4 and AutoDockTools4: Automated docking with selective receptor flexibility. *J Comput Chem.* 2009; 30:2785-91.
9. Wang JC, Lin JH, Chen CM, et al. Robust scoring functions for protein-ligand interactions with quantum chemical charge models. *J Chem Inf Model.* 2011; 51:2528-37.
10. Jakalian A, Jack DB, Bayly CI. Fast, efficient generation of high-quality atomic charges. AM1-BCC model: II. Parameterization and validation. *J Comput Chem.* 2002; 23:1623-41.
11. Wang J, Wolf RM, Caldwell JW, et al. Development and testing of a general amber force field. *J Comput Chem.* 2004; 25:1157-74.
12. Wang J, Wang W, Kollman PA, et al. Automatic atom type and bond type perception in molecular mechanical calculations. *J Mol Graph Model.* 2006; 25:247-60.
13. Humphrey W, Dalke A, Schulten K. VMD: visual molecular dynamics. *J Mol Graph.* 1996; 14:33-8, 27-8.
14. Roe DR, Cheatham TE, 3rd. PTRAJ and CPPTRAJ: Software for Processing and Analysis of Molecular Dynamics Trajectory Data. *J Chem Theory Comput.* 2013; 9:3084-95.